Heliyon 9 (2023) e18603

Contents lists available at ScienceDirect

Heliyon

journal homepage: www.cell.com/heliyon

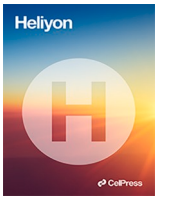

Non-similar solution development for entropy optimized flow of Jeffrey liquid

Tasawar Hayat [a], Aqeela Qaiser [a,*], Shaher Momani [b,c]

[a] Department of Mathematics, Quaid-I-Azam University, 45320, Islamabad, 44000, Pakistan
[b] Department of Mathematics and Science, College of Humanities and Sciences, Ajman University, Ajman, United Arab Emirates
[c] Department of Mathematics, Faculty of Science, University of Jordon, Amman, 11942, Jordan

ARTICLE INFO

Keywords:
Jeffrey fluid model
Mixed convection
Dissipation
Entropy optimization
Non-similar solution

ABSTRACT

Mixed convection in dissipative entropy optimized stagnation point flow of nanomaterial towards stretching Riga sheet is addressed. Brownian and thermophoresis diffusions for nanomaterial are accounted. Constitutive relations for Jeffrey material are utilized. Non-similar solutions for the governing differential systems are developed. OHAM is employed for the convergent series solutions development. Outcomes of pertinent variables on flow quantities of interest are graphically organized. Finally the concluding remarks are arranged.

1. Introduction

Materials subject to rheological characteristics are now acknowledged very useful in the industrial processes. Diverse characteristics of several materials lead to many models with rheological characteristics. Jeffrey liquid is one of such materials exhibiting both relaxation and retardation times. Attention to Jeffrey liquid has been focused in the past. For instance Hayat and Mustafa [1] examined radiative flow of Jeffrey liquid. Nadeem et al. [2] have studied unsteady oscillatory flow of Jeffery fluid with stagnation point. Hayat et al. [3] addressed flow in presence of heat source and porous space. Shehzad et al. [4] addressed Joule heating impact in flow of Jeffrey nanomaterial. Khan [5] discussed unsteady free convection flow of Jeffrey material. Forced convection flow of Jeffrey liquid is explored by Dalir [6] Idowu et al. [7] examined MHD chemically reactive flow of Jeffrey liquid.

Flow subject to entropy generation is motivated by the recent researchers. In fact the development in research has found the point that even if energy being preserved but the quality of energy will be lost when it is entropy generated. Entropy generation is very important in the process for the conversion of heat transportation, solar and storage thermal power, solar collectors, heat exchanger, chemical vapor deposition devices etc. Bejan [8] made fundamental contribution in this direction. Dissipation and entropy generation in Cross fluid flow are addressed by Khan and Ali [9] Entropy in MHD peristaltic flow of nanomaterial is due to Rashidi et al. [10]. Ali et al. [11] studied entropy generation in flow of Cross nanofluid. Electrosmotic flow with entropy is discussed by Ranjit and Shit [12]. Further information on the topic can be mentioned in Refs. [13–17].

This communication aims for mixed convective stagnation point flow by a Riga sheet with dissipation. Entropy generation is also explored. Nanofluid model with Brownian movement and thermophoresis is chosen. Rheological features for Jeffrey fluid are considered. Non-similar solutions to nonlinear problems are constructed. The solutions are analyzed for emerging sundry parameters.

* Corresponding author.
E-mail address: aqeelaqaiser@math.qau.edu.pk (A. Qaiser).

https://doi.org/10.1016/j.heliyon.2023.e18603
Received 19 February 2023; Received in revised form 22 July 2023; Accepted 22 July 2023
Available online 27 July 2023

Nomenclature

u, v	x, y Velocity components
$\mathbf{J}, \mathbf{q}$	Mass flux, Heat flux
T, C	Temperature, Concentration
T_w, C_w	Surface Temperature, Surface Concentration
T_∞, C_∞	Ambient Temperature, Ambient Concentration
U_∞	Ambient velocity
A	First Rivilin Erickson Tensor
a, c	Rate Constants
k_f	Thermal conductivity
ν_f	Viscosity
J_o	Current Density
g	Gravity
λ_1	Ratio of Relaxation and Retardation Times
λ_2	Mixed Convection Parameter
λ_3	Buoyancy Ratio Parameter
λ_4	Retardation time
λ_6	Diffusion Parameter
S	Parameter for Ratio of Rates
D_B, D_T	(Brownian motion, Thermopherotic Diffusion) Coefficients
α_f	Thermal Diffusivity
M	Modified Hartmman Number
$\tau\left(=\frac{(\rho C_p)_p}{(\rho C_f)_f}\right)$	Heat Capacity Ratio
ψ	Stream Function
$(\rho C)_f$	Heat Capacity of Fluid
β	Deborah Number
Pr	Prandtl Number
Ec	Eckert Number
Sc	Schmidt Number
Br	Brikmann Number
Re	Reynold Number
τ_{xy}	Wall Shear Stress
q_w	Heat Flux at Wall
q_m	Surface Mass Flux
$f^{'}, t, J$	Dimensionless Velocity, Temperature, Concentration
γ_3	Concentration Difference Parameter
Ω	Temperature Difference Parameter
N_s	Entropy Generation
C_f	Coefficient of skin Friction
Nu	Nusselt Number
Sh	Sherwood Number
B	Non-Dimensional Parameter
δ	Heat Generation Parameter
β_t	Material Parameter
R, D	Gas constant, Diffusion Coefficient

2. Modelling

Two-dimensional flow of Jeffrey liquid due to Riga stretching surface is addressed. Brownian and thermophoresis diffusions are present. The sheet is stretching along $(x-axis)$ with velocity $(u_w = ax)$ where $a > 0$ being stretching rate. Here $(u_e = cx)$ denotes velocity away from the surface, T_w surface temperature and T_∞ ambient temperature. Under such considerations the governing expressions are [1–6]

$$\frac{\partial u}{\partial x} = -\frac{\partial v}{\partial y} \tag{1}$$

$$\rho\left(u\frac{\partial u}{\partial x}+v\frac{\partial u}{\partial y}\right)=\frac{\mu}{1+\lambda_1}\left(\frac{\partial^2 u}{\partial y^2}+\lambda_4\left(\frac{\partial u}{\partial y}\frac{\partial^2 u}{\partial x\partial y}+u\frac{\partial^3 u}{\partial x\partial y^2}-\frac{\partial u}{\partial x}\frac{\partial^2 u}{\partial y^2}+v\frac{\partial^3 u}{\partial y^3}\right)\right)$$
$$+\rho U_\infty\frac{\partial U\infty}{\partial x}+\frac{\pi J_o Q_o}{8}\exp\left(-\frac{\pi}{a_1}y\right)+\rho g\beta_t(T-T_\infty)+\rho g\beta_c(C-C_\infty)\Bigg\} \tag{2}$$

$$v\frac{\partial T}{\partial y}+u\frac{\partial T}{\partial x}=\frac{k}{\rho c_p}\frac{\partial^2 T}{\partial y^2}+\frac{\upsilon}{c_p(1+\lambda_1)}\left\{\left(\frac{\partial u}{\partial y}\right)^2+\lambda_4\left(v\frac{\partial u}{\partial y}\frac{\partial^2 u}{\partial y^2}+u\frac{\partial u}{\partial y}\frac{\partial^2 u}{\partial x\partial y}\right)\right\}$$
$$+\frac{\rho c_p}{\rho c_f}\left(D_B\frac{\partial T}{\partial y}\frac{\partial C}{\partial y}+\frac{D_T}{T_\infty}\left(\frac{\partial T}{\partial y}\right)^2\right)\Bigg\} \tag{3}$$

$$v\frac{\partial C}{\partial y}+u\frac{\partial C}{\partial x}=\frac{D_T}{T_\infty}\frac{\partial^2 T}{\partial y^2}+D_B\frac{\partial^2 C}{\partial y^2} \tag{4}$$

The relevant boundary conditions are

$$\left.\begin{array}{l} u=u_w=ax, v=0, T=T_w, C=C_w \quad \text{at } y=0 \\ u\to U_\infty=cx, T\to T_\infty, C\to C_\infty \quad \text{as } y\to\infty \end{array}\right\}. \tag{5}$$

3. Non-similar solutions

By considering transformations

$$\left.\begin{array}{l} u=cxf'(\xi,\eta), v=-\sqrt{c\nu}\left(f+\xi\dfrac{\partial f}{\partial\xi}\right), \eta=\sqrt{\dfrac{c}{\nu}}y, \\ \Psi=\sqrt{a\nu}xf'(\xi,\eta), C=\dfrac{T-T_\infty}{T_w-T_\infty}, J=\dfrac{C-C_\infty}{C_w-C_\infty}, \xi=\dfrac{x}{L} \end{array}\right\} \tag{6}$$

we arrive at

$$f'''+\beta\left(f''^2-ff^{iv}\right)+(1+\lambda_1)\left(ff''-f'^2\right)+\frac{M}{\xi}(1+\lambda_1)\exp(-B\eta)+(1+\lambda_1)S^2$$
$$+\frac{\lambda_2(1+\lambda_1)}{\xi}t+\frac{\lambda_3(1+\lambda_1)}{\xi}J=(1+\lambda_1)(\xi f^{*'}-\xi f''f^*)+\beta\left(\xi f'''f^{*'}-\xi ff^{*'''}+\xi f^{iv}f^*\right)\Bigg\} \tag{7}$$

$$\frac{1}{\Pr}t''+t'f+\frac{(Ec)\,\xi^2}{1+\lambda_1}*\left[f''^2+\beta\left(f'f''^2-ff''f'''\right)\right]+N_Bt'J'+N_tt'^2=\xi f't^*-t'\xi f^*$$
$$-\frac{(Ec)\,(\beta)\,\xi^3}{1+\lambda_1}\left(f'f''f^{*}-f''f'''f^*\right)\Bigg\} \tag{8}$$

$$J''+(Sc)fJ'+\frac{N_t}{N_B}t''=(Sc)\xi(f'J^*-J'f^*) \tag{9}$$

$$\left.\begin{array}{l} f'(0)=1, f'(\infty)=S, f(0)=-\xi\dfrac{\partial f}{\partial\xi} \\ t(0)=1, t(\infty)=0 \\ J(0)=1, J(\infty)=0 \end{array}\right\} \tag{10}$$

3.1. First order of truncation

In first order of truncation, the terms including $\frac{\partial(.)}{\partial\xi}$ are assumed very small and may be approximated by zero. Hence one can write

$$\left.\begin{array}{l} f'''+(1+\lambda_1)\left(ff''-f'^2\right)+\beta\left(f''^2-ff^{iv}\right)+(1+\lambda_1)S^2+ \\ \dfrac{M}{\xi}(1+\lambda_1)\exp(-B\eta)+\dfrac{\lambda_2}{\xi}(1+\lambda_1)t+\dfrac{\lambda_3}{\xi}(1+\lambda_1)J=0 \end{array}\right\} \tag{11}$$

$$\frac{1}{\Pr}t''+t'f+\frac{(Ec)\,\xi^2}{1+\lambda_1}\left(f'f''^2-ff''f'''\right)+N_Bt'J'+N_tt'^2=0 \tag{12}$$

$$J''+(Sc)fJ'+\frac{N_t}{N_B}t''=0 \tag{13}$$

$$\left.\begin{array}{c} f'(0)=1, f'(\infty)=S, f'(0)=0 \\ t(0)=1, t(\infty)=0 \\ J(0)=1, J(\infty)=0 \end{array}\right\} \tag{14}$$

3.2. Second order of truncation

We here write

$$f^*=\frac{\partial f}{\partial \xi}, t^*=\frac{\partial t}{\partial \xi}, J^*=\frac{\partial J}{\partial \xi}, \tag{15}$$

and express that

$$\left.\begin{array}{c} f'''+(1+\lambda_1)(ff^{*'}+f''f^*-2f'f^{*'})+\beta\left(2f''f^{*''}-ff^{iv*}-f^{iv}f^*\right) \\ -\frac{M}{\xi^2}(1+\lambda_1)\exp(-B\eta)-\frac{\lambda_2}{\xi^2}(1+\lambda_1)t+\frac{\lambda_2}{\xi}(1+\lambda_1)t^*-\frac{\lambda_3}{\xi^2}(1+\lambda_1)J \\ +\frac{\lambda_3}{\xi}(1+\lambda_1)J^*=(1+\lambda_1)(f'f^{*'}-f^*f''-\xi f^{*''}f^*)+\beta\left(f'''f^{*'}+\xi f^{*'''}f^{*'}\right. \\ \left.-ff^{*'''}-\xi f^*f^{*'''}+f^{iv}f^*+\xi f^{*iv}f^*\right\} \end{array}\right. \tag{16}$$

$$\left.\begin{array}{c} \frac{1}{\Pr}t^{*'}+ft^{*'}+f^{*'}t'+2\xi\frac{Ec}{1+\lambda_1}\left[f''^2+\beta\left(f'f''^2-ff''f'''\right)\right]+\frac{Ec\xi^2}{1+\lambda_1}\left[2f''f^{*''}+\beta\left(2f'f''f^{*''}+f''^2f^{*'}-f^*f''f'''-ff^{*''}f'''-ff''f^{*'''}\right)\right] \\ +N_Bt^{*'}J'+N_Bt'J^{*'}+2N_tt't'^*=f't^{*'}+\xi f^{*'}t^*-\xi t^{*'}f^*-t'f^*-\frac{\beta Ec\xi^3}{1+\lambda_1}\left(f^{*'}f'f^{*''}+f'f^{*'2}-f^{*''}f''f^*-f''f^{*''}f^*\right)-\frac{3\beta Ec\xi^2}{1+\lambda_1}(f'f''f^{*''}-f''f'''f^*) \quad \} \end{array}\right. \tag{17}$$

$$J^{*'}+ScJ^{*'}f+Scf^*J'+\frac{N_t}{N_B}t^{*''}=Sc(f'J^*-J'f^*+\xi(f^{*'}J^*-J^{*'}f^*))\Big\} \tag{18}$$

$$\left.\begin{array}{c} f^{*'}(0)=0, f^{*'}(\infty)=0, f^{*'}(0)=0 \\ t^*(0)=0, t^*(\infty)=0 \\ J^*(0)=0, J^*(\infty)=0 \end{array}\right\} \tag{19}$$

4. Physical quantities

The following definitions for skin friction coefficient (C_f) and local Nusselt and Sherwood numbers hold

$$C_f=\frac{\tau_w}{\rho u_w^2}, Nu_x=\frac{xq_w}{k(T_w-T_\infty)}, Sh_x=\frac{xc_w}{D_B(C_w-C_\infty)} \tag{20}$$

where the wall shear stress (τ_w), heat flux (q_w) and mass flux (c_w) have been expressed by

$$\left.\begin{array}{c} \tau_w=\frac{\mu}{1+\lambda_1}\left(\frac{\partial u}{\partial y}+\lambda_4\left(u\frac{\partial^2 u}{\partial x\partial y}+v\frac{\partial^2 u}{\partial y^2}\right)\right)_{y=0} \\ q_w=-k\left(\frac{\partial T}{\partial y}\right)_{y=0}, c_w=-D_B\left(\frac{\partial C}{\partial y}\right)_{y=0} \end{array}\right\} \tag{21}$$

Dimensionless forms of $(C_f), (Nu_x)$ and (Sh_x) are given below

$$(C_f)\ (\mathrm{Re})^{1/2}=\frac{1}{1+\lambda_1}\left(f''(0)+\beta\left(f'(0)f''(0)-f(0)f'''(0)+\xi f'(0)\ \frac{\partial f''}{\partial \xi}-\xi f'''(0)\ \frac{\partial f}{\partial \xi}\right)\right) \tag{22}$$

$$(\mathrm{Re})^{-1/2}Nu_x=-\xi t'(0) \tag{23}$$

$$(\mathrm{Re})^{-1/2}Sh_x=-\xi J'(0). \tag{24}$$

5. Entropy generation

By definition one has [17].

Table: 1
Individual average squared residual errors.

k^*	$\varepsilon^f_{k^*}$	$\varepsilon^t_{k^*}$	$\varepsilon^J_{k^*}$
2	0.0462563	0.012580	0.1475
6	0.0393521	0.00236675	0.0172569
10	0.0326185	0.000245317	0.0055238
14	0.0295632	0.0000456789	0.00114646
16	0.0282456	0.000056883	0.00053328

$$N_s = \frac{s_{gen}}{(s_{gen})} \tag{25}$$

$$S_{gen} = \frac{k}{T_\infty^2}\left(\frac{\partial T}{\partial y}\right)^2 + \frac{\mu}{T_\infty(1+\lambda_1)}\left[\left(\frac{\partial u}{\partial y}\right)^2 + \lambda_2\left(u\frac{\partial u}{\partial y}\frac{\partial^2 u}{\partial x \partial y} + v\frac{\partial u}{\partial y}\frac{\partial^2 u}{\partial y^2}\right)\right] + \frac{RD}{T_\infty}\left(\frac{\partial T}{\partial y}\frac{\partial C}{\partial y}\right) + \frac{RD}{C_\infty}\left(\frac{\partial C}{\partial y}\right)^2\Bigg\} \tag{26}$$

$$(S_{gen})_o = \frac{k(\Delta T)^2}{\xi^2 L^2 T_\infty^2} \tag{27}$$

above expressions yield

$$N_s = \mathrm{Re}\xi^2 t'^2 + \frac{Br\mathrm{Re}\xi^4}{\Omega(1+\lambda_1)}\left[f''^2 + \beta(f'f''' - ff''f''' + f'f''f^{*''} - f''f'''f^{*'})\right] + \frac{\mathrm{Re}\lambda_6\gamma_3}{\Omega}t'J' + \mathrm{Re}\lambda_6\gamma_3 J'^2\Bigg\}. \tag{28}$$

Dimensionless parameters are

$$\left.\begin{aligned} &\beta = \lambda_4 c, S = \frac{a}{c}, M = \frac{\pi J_o Q_o}{8\rho c^2 L}, B = \frac{\pi}{a_1}\sqrt{\frac{\nu}{c}}, \lambda_2 = \frac{g\beta_t(T_w - T_\infty)}{c^2 L}, \\ &\lambda_3 = \frac{g\beta c(C_w - C_\infty)}{c^2 L}, \mathrm{Pr} = \frac{\nu\rho c_p}{k}, Ec = \frac{c^2 L^2}{c_\rho(T_w - T_\infty)}, N_B = \frac{\tau D_B(C_w - C_\infty)}{\nu}, \\ &N_t = \frac{\tau D_T(T_w - T_\infty)}{\nu T_\infty}, Sc = \frac{\nu}{D_B}, \lambda_6 = \frac{RD(C_w - C_\infty)}{k}, \gamma_3 = \frac{\Delta C}{C_\infty}, \\ &\mathrm{Re} = \frac{cL^2}{\nu}, Br = \frac{\mu c^2 L^2}{k\Delta T}, \Omega = \frac{\Delta T}{T_\infty}, \end{aligned}\right\} \tag{29}$$

6. Solutions by OHAM

For optimal homotopy analysis method (OHAM) the linear operators and initial approximations may be expressed as follows:

$$\begin{aligned} &f_0(\xi) = (S\xi) + (1-S)\left(1 - e^{-\xi}\right), \\ &\theta_0(\xi) = e^{-\xi}, \\ &j_0(\xi) = e^{-\xi}, \end{aligned} \tag{30}$$

$$\mathbf{L}_f(f) = f''' - f', \mathbf{L}_t(t) = t'' - t, \mathbf{L}_J(J) = J'' - J \tag{31}$$

Properties satisfied by the operators are

$$\mathbf{L}_f\left[A_1 + A_2 e^{\xi} + A e^{-\xi}\right] = 0 \tag{32}$$

$$\mathbf{L}_t\left[A_4 e^{\xi} + A_5 e^{-\xi}\right] = 0 \tag{33}$$

$$\mathbf{L}_J\left[A_6 e^{\xi} + A_7 e^{-\xi}\right] = 0 \tag{34}$$

in which $A_i (i = 1-7)$ are the constants. Average squared residual errors are [18–24].

$$\varepsilon^J_{k^*}(h_f) = \frac{1}{N+1}\sum_{j=0}^{N}\left[\sum_{i=0}^{k^*}(f_i)_{\xi = j\Pi\eta},\right]^2 \tag{35}$$

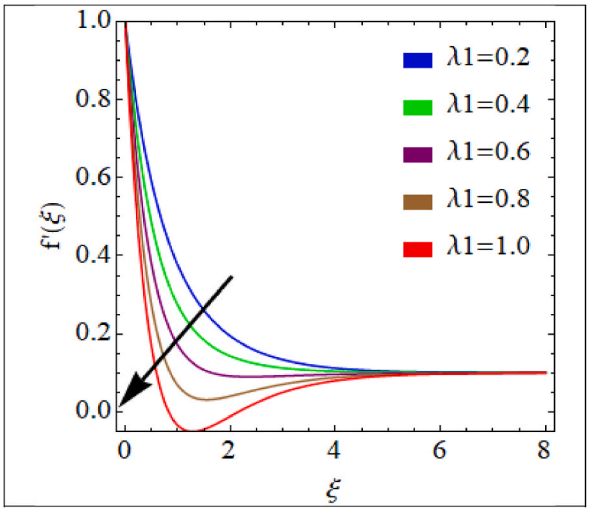

Fig. 1. Behaviour of λ_1 on $f^{'}(\xi)$.

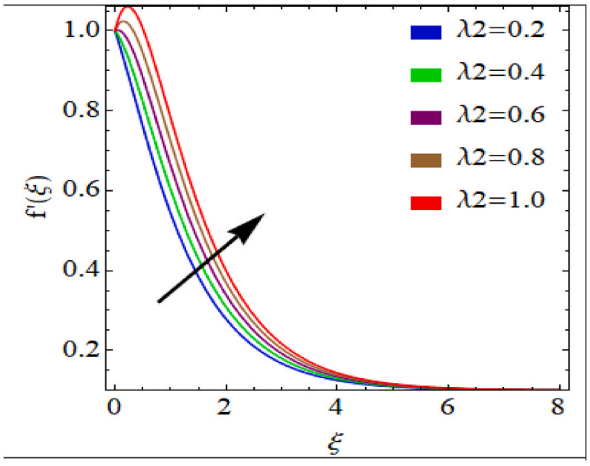

Fig. 2. Behaviour of λ_2 on $f^{'}(\xi)$.

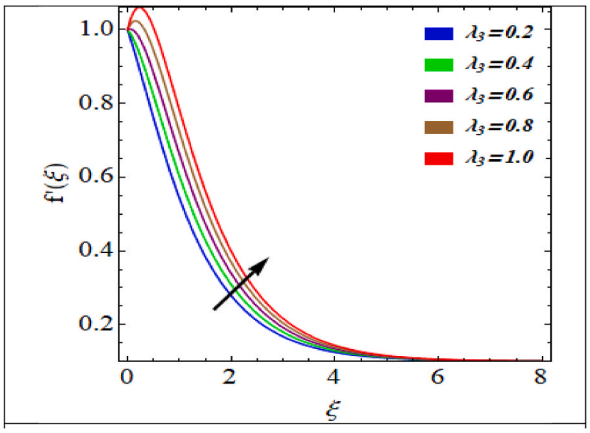

Fig. 3. Behaviour of λ_3 on $f^{'}(\xi)$.

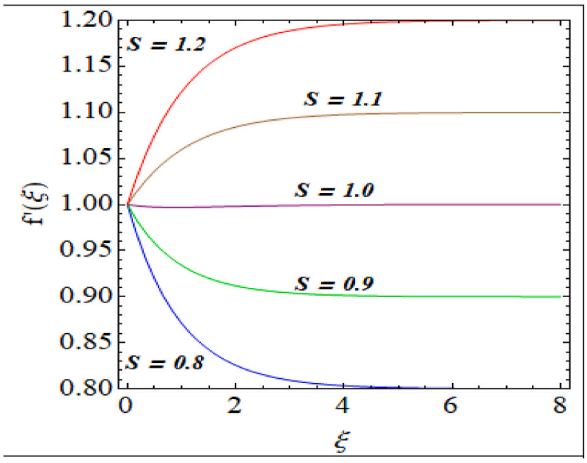

Fig. 4. Behaviour of S on $f'(\xi)$.

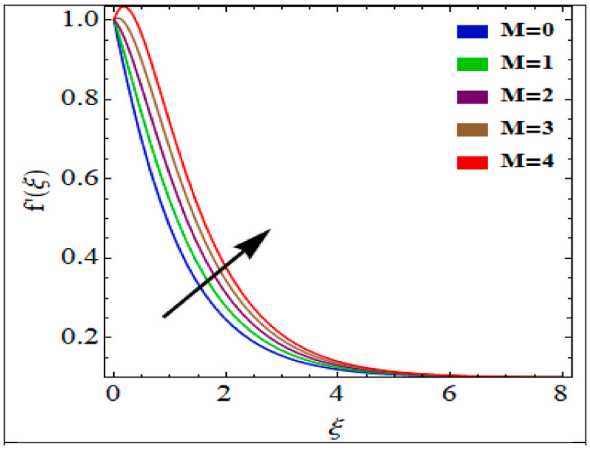

Fig. 5. Behaviour of M on $f'(\xi)$.

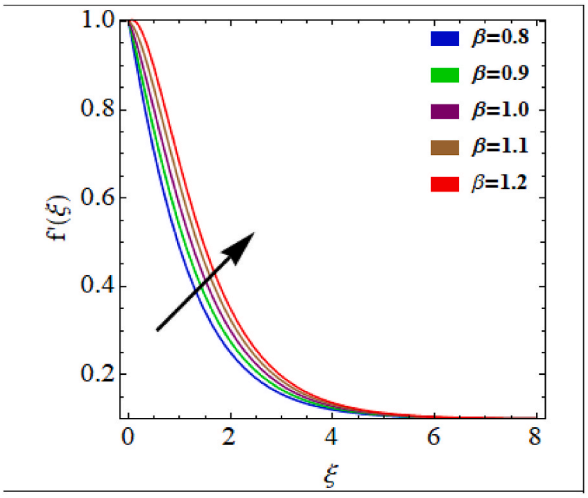

Fig. 6. Behaviour of β on $f'(\xi)$.

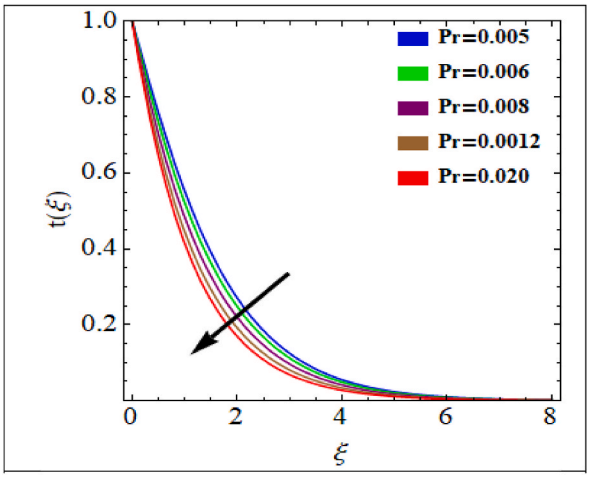

Fig. 7. Behaviour of Pr on $t(\xi)$.

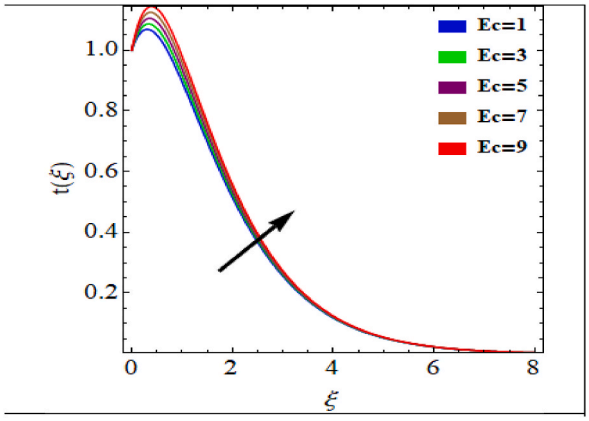

Fig. 8. Behaviour of *Ec* on $t(\xi)$.

$$\varepsilon_{k^*}^{J}\left(h_f,h_t,h_J\right)=\frac{1}{N+1}\sum_{j=0}^{N}\left[\sum_{i=0}^{k^*}\left(f_i\right)_{\xi=j\Pi\eta},\sum_{i=0}^{k^*}\left(t_i\right)_{\xi=j\Pi\eta},\sum_{i=0}^{k^*}\left(J_i\right)_{\xi=j\Pi\eta}\right]^2 \tag{36}$$

$$\varepsilon_{k^*}^{J}\left(h_f,h_t,h_J\right)=\frac{1}{N+1}\sum_{j=0}^{N}\left[\sum_{i=0}^{k^*}\left(f_i\right)_{\xi=j\Pi\eta},\sum_{i=0}^{k^*}\left(t_i\right)_{\xi=j\Pi\eta},\sum_{i=0}^{k^*}\left(J_i\right)_{\xi=j\Pi\eta}\right]^2 \tag{37}$$

subject to total squared residual error

$$\varepsilon_{k^*}^{t^*}=\varepsilon_{k^*}^{f}+\varepsilon_{k^*}^{t}+\varepsilon_{k*}^{J}, \tag{38}$$

with convergence control variables $h_f=-1.23589, h_\theta=-0.623586, h_g=-1.452368$ and $\varepsilon_{k^*}^{t^*}=0.0568521$.Table 1 elucidates such residual. The values in errors reduce for higher order approximation.

7. Discussion

Fig. 1 shows velocity against (λ_1). Here velocity against (λ_1) is reduced. Retardation time has an inverse relationship with (λ_1). Fig. 2 highlights velocity impact for (λ_2).The fluid velocity is seen to rise for increasing (λ_2). Characteristic of velocity against buoyancy parameter (λ_3) has been shown through Fig. 3. The velocity versus (λ_3) enhances. Fig. 4 indicates outcome of (S) on $f'(\xi)$. Velocity enhances as the ratio parameter highers. Fig. 5 illustrates velocity for modified Hartmann number (M). Higher (M) reduce the velocity. Behavior of (β) on $f'(\xi)$ has been clarified in Fig. 6. Velocity through this sketch is enhanced when (β) highers. Fig. 7 displays the temperature through (Pr). It is evident that when Prandtl number rises then fluid temperature reduces. Fig. 8 shows variation in

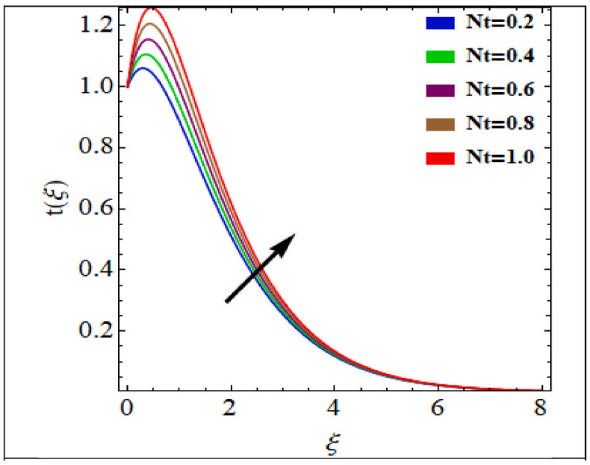

Fig. 9. Behaviour of *Nt* on $t(\xi)$.

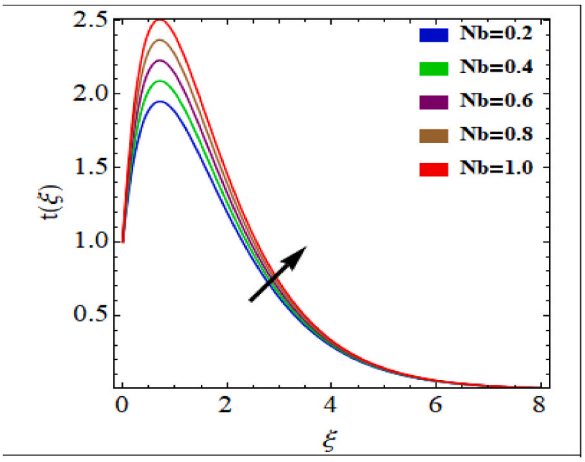

Fig. 10. Behaviour of *Nb* on $t(\xi)$.

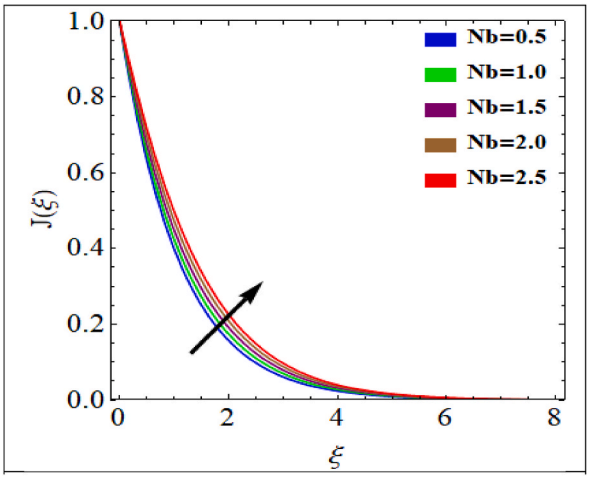

Fig. 11. Behaviour of *Nb* on $J(\xi)$.

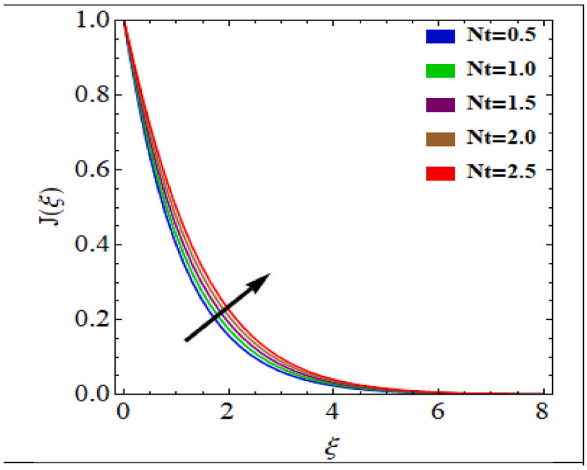

Fig. 12. Behaviour of *Nt* on $J(\xi)$.

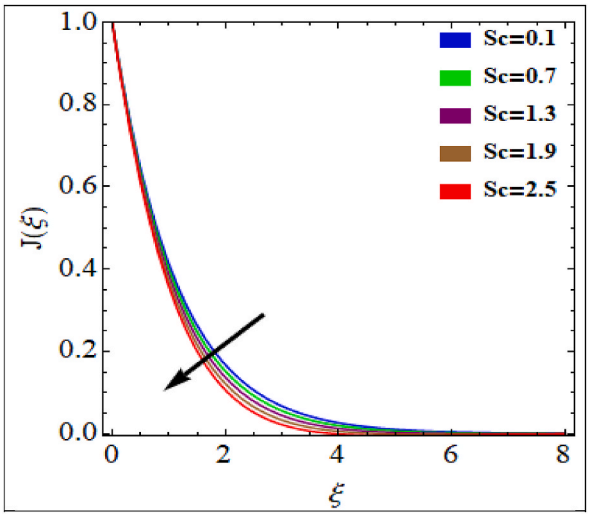

Fig. 13. Behaviour of *Sc* on $J(\xi)$.

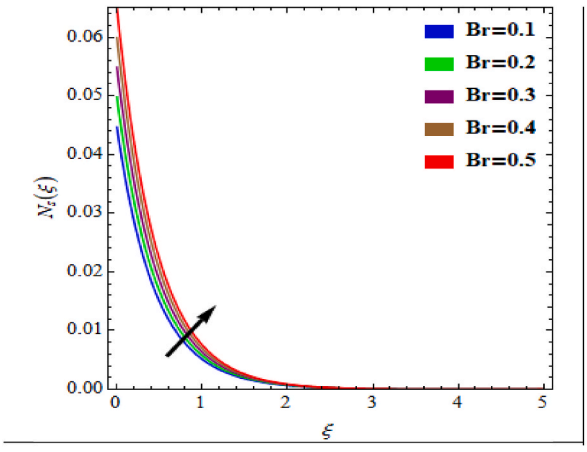

Fig. 14. Behaviour of *Br* on $N_s(\xi)$.

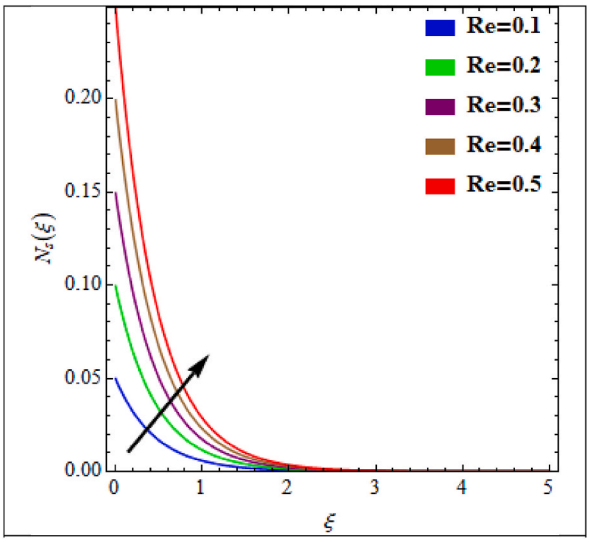

Fig. 15. Behaviour of Re on $N_s(\xi)$.

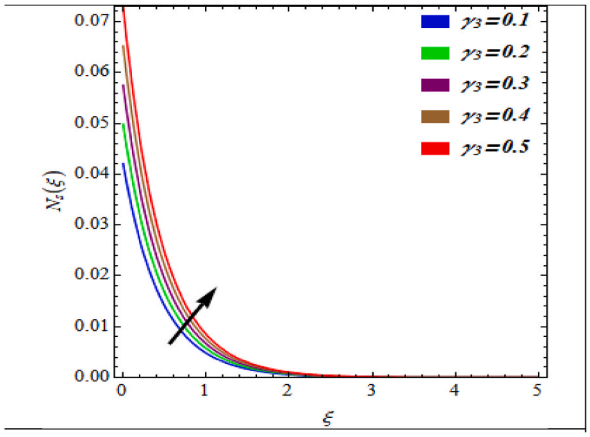

Fig. 16. Behaviour of γ_3 on $N_s(\xi)$.

temperature for Eckert number (Ec). As expected a rise in temperature is observed for higher (Ec). Temperature for thermophoresis parameter (Nt) is depicted in Fig. 9. Infact nanoparticles move from a hot region to cool zone and therefore temperature enhances. Temperature variation versus Brownian motion parameter (Nb) can be seen in Fig. 10. Higher temperature is noticed with increasing (Nb). Fig. 11 showed a significant reduction in concentration when the Brownian motion parameter (Nb) increases. Distribution of concentration versus (Nt) is sketched in Fig. 12. Higher value of parameter (Nt) yield stronger concentration. Fig. 13 plotted concentration for Schmidt number (Sc). Brownian diffusion coefficient and Schmidt number have inverse relationship. Concentration layer thickness is thinner and wall concentration gradient is higher for larger Schmidt number (Sc). Entropy generating rate (N_s) for varying (Br) is shown in Fig. 14. For higher values of (Br) the entropy enhances. (N_s) against Reynolds number (Re) is given in Fig. 15. It can be shown that high Reynolds number causes increase in entropy generation rate. Effect of concentration difference parameter (γ_3) on (N_s) is described in Fig. 16. Larger values of (γ_3) enhance entropy generation rate (N_s). Fig. 17 plots temperature difference parameter (Ω) on (N_s). Higher level of disorderedness result in reduction of (N_s) against (λ_6) in Fig. 18. Here entropy rate increases with higher values of (λ_6).

8. Concluding remarks

The worth mentioning points are given below.

F0B7 Opposite trend of velocity for λ_1 is noticed when compared with λ_2 and λ_3.
F0B7 Velocity for M and S has opposite scenario.

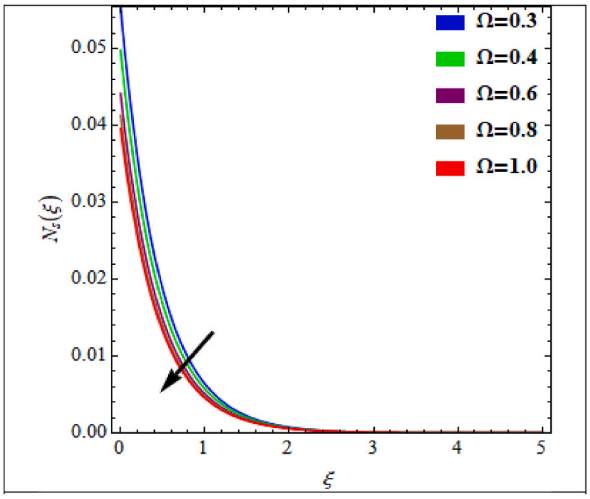

Fig. 17. Behaviour of Ω on $N_s(\xi)$.

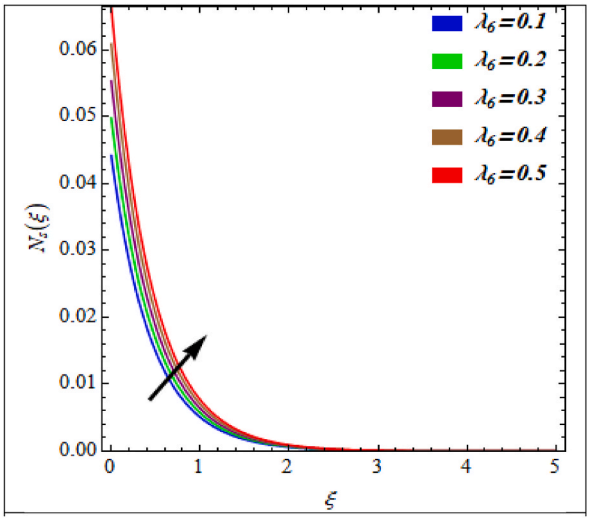

Fig. 18. Behaviour of λ_6 on $N_s(\xi)$.

F0B7 Temperature $t(\xi)$ is reduced for Prandtl number (Pr) while opposite holds for Eckert number (Ec).
F0B7 Concentration $J(\xi)$ is increased against (N_B) and (Nt) while reverse holds for (Sc).
F0B7 Local Reynolds number (Re) and (γ_3) enhance ($N_s(\xi)$).

Author contribution statement

Tasawar Hayat, Aqeela Qaiser: Conceived and designed the analysis; Analyzed and interpreted the data; Wrote the paper. Shaher Momani: Contributed analysis tools or data.

Data availability statement

Data will be made available on request.

Declaration of competing interest

The authors declared that they have no conflict of interest and the paper presents their own work which does not been infringe any third-party rights, especially authorship of any part of the article is an original contribution, not published before and not being under consideration for publication elsewhere.

References

[1] T. Hayat, M. Mustafa, Influence of thermal radiation on the unsteady mixed convection flow of a Jeffrey fluid over a stretching sheet, Z. Naturforsch. 65 (2010) 711–719.
[2] S. Nadeem, B. Tahir, F. Labropulu, N.S. Akbar, Unsteady oscillatory stagnation point flow of a Jeffrey fluid, J. Aero. Eng. 27 (2014) 636–643.
[3] T. Hayat, S.A. Shehzad, M. Qasim, S. Obaidat, Radiative flow of Jeffery fluid in a porous medium with power law heat flux and heat source, Nucl. Eng. Des. 243 (2012) 15–19.
[4] S.A. Shehzad, A. Alsaedi, T. Hayat, Influence of thermophoresis and Joule heating on the radiative flow of Jeffrey fluid with mixed convection, Braz. J. Chem. Eng. 30 (2013) 897–908.
[5] I. Khan, A note on exact solutions for the unsteady free convection flow of a Jeffrey fluid, Z. Naturforschung A 70 (2015) 272–284.
[6] T. Hayat, M. Khan, K. Fakhar, N. Amin, Oscillatory rotating flows of a fractional Jeffrey fluid filling a porous space, J. Porous Media 13 (2010) 29–38.
[7] A.S. Idowu, K.M. Joseph, S. Daniel, Effect of heat and mass transfer on unsteady MHD oscillatory flow of Jeffrey fluid in a horizontal channel with chemical reaction, IOSR J. Math. 8 (2013) 74–87.
[8] A. Bejan, Entropy generation minimization: the new thermodynamics of finite-size devices and finite-time processes, J. Appl. Phys. 79 (1996) 1191–1218.
[9] W.A. Khan, M. Ali, Recent developments in modelling and simulation of entropy generation for dissipative cross material with quartic auto catalyst, Appl. Phys. A 125 (2019) 397.
[10] M.M. Rashidi, M.M. Bhatti, M.A. Abbas, M.E.S. Ali, Entropy generation on MHD blood flow of nanofluid due to peristaltic waves, Entropy 18 (2016) 117.
[11] M. Ali, W.A. Khan, M. Irfan, F. Sultan, M. Shahzed, M. Khan, Computational analysis of entropy generation for cross-nanofluid flow, Appl. Nanosci. (2019) 428–433.
[12] N.K. Ranjit, G.C. Shit, Entropy generation on electroosmotic flow pumping by a uniform peristaltic wave under magnetic environment, Energy 128 (2017) 649–660.
[13] U. Khan, A. Zaib, A. Ishak, Magnetic field effect on Sisko fluid flow containing gold nanoparticles through a porous curved surface in the presence of radiation and partial slip, Mathematics 9 (2021) 921.
[14] U. Khan, A. Zaib, S. Abu Bakar, A. Ishak, Stagnation-point flow of a hybrid nanoliquid over a non-isothermal stretching/shrinking sheet with characteristics of inertial and microstructure, Case Stud. Therm. Eng. (2021), 101150.
[15] U. Khan, A. Zaib, A. Ishak, I. Waini, I. Pop, S. Elattar, A.M. Abed, Stagnation point flow of a water-based graphene-oxide over a stretching/shrinking sheet under an induced magnetic field with homogeneous-heterogeneous chemical reaction, J. Magn. Magn Mater. (2023), 170287.
[16] U. Khan, A. Zaib, A. Ishak, S.M. Eldin, A.M. Alotaibi, Z. Raizah, I. Waini, S. Elattar, A.M. Abed, Features of hybridized AA7072 and AA7075 alloys nanomaterials with melting heat transfer past a movable cylinder with Thompson and Troian slip effect, Arab. J. Chem. (2023), 104503.
[17] N. Dalir, Numerical study of entropy generation for forced convection flow and heat transfer of a Jeffrey fluid over a stretching sheet, Alex. Eng. J. (2014) 769–778.
[18] S.J. Liao, Homotopy Analysis Method in Non-linear Differential Equations, Springer and Higher Education Press, Heidelberg, 2012.
[19] L. Zheng, L. Wang, X. Zhang, Analytic solutions of unsteady boundary flow and heat transfer on a permeable stretching sheet with non-uniform heat source/sink, Commun. Nonlinear Sci. Numer. Simul. 16 (2011) 731–740.
[20] M.A. Sadiq, F. Haider, T. Hayat, A. Alsaedi, Partial slip in Darcy-Forchheimer carbon nanotubes flow by rotating disk, Int. Commun. Heat Mass Transf. 116 (2020), 104641.
[21] J. Zhu, D. Yang, L. Zheng, X. Zhang, Effects of second order velocity slip and nanoparticles migration on flow of Buongiorno nanofluid, Appl. Math. Lett. 52 (2016) 183–191.
[22] A. Al-Qudah, Z. Odibat, N. Shawagfeh, An optimal homotopy analysis transform method for handling nonlinear PDEs, Int. J. Appl. Comput. Math. 8 (2022) 260.
[23] U. Biswal, S. Chakraverty, Investigation of Jeffery-Hamel flow for nanofluid in the presence of magnetic field by a new approach in the optimal homotopy analysis method, J. Appl. Comput. Mech. 8 (2022) 48–59.
[24] E. Seid, E. Haile, T. Walelign, Multiple slip, Soret and Dufour effects in fluid flow near a vertical stretching sheet in the presence of magnetic nanoparticles, Int. J. Thermofluids 13 (2022), 100136.